Vacuum ultraviolet spectroscopy in detached plasmas with impurity gas seeding in LHD

Vacuum ultraviolet spectroscopy in detached plasmas with impurity gas seeding in LHD

C. Suzuki[a*], I. Murakami[a], T. Akiyama[a], S. Masuzaki[a], H. Funaba[a], M. Yoshinuma[a], LHD Experiment Group[a]

[a]*National Institute for Fusion Science, 322-6 Oroshi-cho, Toki 509-5292, Japan*

Abstract

We have carried out vacuum ultraviolet (VUV) spectroscopy of impurity ions in detached plasmas with impurity gas seeding in the Large Helical Device (LHD). In neon (Ne) gas seeding experiments, temporal evolutions of VUV spectral lines from Ne IV–VIII were recorded by a grazing incidence spectrometer. In addition, spatial profiles of fully ionized Ne density were measured by charge exchange spectroscopy. An electron temperature range where each ion emits is inferred based on the comparisons of the measured line intensity ratios with the calculations using collisional-radiative models.

PACS: 32.30.Jc, 32.70.Fw, 52.25.Vy, 52.55.Hc

PSI-20 keywords: Collisional-radiative model, Detached plasma, Impurity seeding, LHD, Spectroscopy

*Corresponding author address: National Institute for Fusion Science, 322-6 Oroshi-cho, Toki 509-5292, Japan

*Corresponding author E-mail: csuzuki@nifs.ac.jp

Presenting author: Chihiro Suzuki

Presenting author e-mail: csuzuki@nifs.ac.jp

1. Introduction

Impurity gas seeding is one of the promising scenarios to mitigate divertor heat loads through the enhanced radiation power in edge plasmas. In this context, nitrogen (N_2), neon (Ne), and argon (Ar) gas seeding experiments have widely been carried out in tokamaks until now [1–4]. In JT-60U, for example, Ar and Ne gasses were injected into H-mode plasmas and large enhancement of radiated power and reduction of heat load could be achieved without significant degradation of confinement [1].

In the last few years, impurity gas seeding experiments have been extensively performed also in the Large Helical Device (LHD) to achieve the divertor detachment [5]. The Ne gas seeding experiment in LHD has demonstrated that the divertor heat load was reduced without serious degradation of plasma confinement up to the radiation enhancement factor of P_{rad}/P_{NBI} ~0.3, where P_{rad} and P_{NBI} denote the total radiated power and the neutral beam injection (NBI) heating power, respectively. In addition to N_2, Ne, and Ar gasses, a krypton (Kr) gas seeding experiment has recently been launched in LHD to explore the possibility of more radiation enhancement from high Z impurity ions.

Radiation from the seeded impurity ions in the vacuum ultraviolet (VUV) wavelength region may largely contribute to the total radiated power in these experiments. Therefore, VUV spectroscopy would be helpful to determine which charge states emit dominantly, where they emit the radiation, and how much they contribute to the total radiated power. In JT-60U, VUV spectroscopy has been applied to Ne seeded plasmas using absolutely calibrated VUV spectrometer [6,7], and the contributions from each ion stage of Ne and intrinsic carbon to the total radiated power have been successfully estimated from the detailed analyses of line intensities from Ne ions based on the atomic modeling [7].

Considering its usefulness, we have launched VUV spectroscopy in the impurity seeding experiments in LHD to observe temporal evolutions of line intensities from a wide range of

impurity ion stages. We report on the recent results on Ne seeded plasmas in this article. Though the absolute sensitivity of the spectrometer used in this study has not been calibrated yet, detailed information on profiles of electron temperature and fully ionized Ne density is available in LHD. Therefore, it is still possible to compare the measurements with theoretical calculations.

2. Experiment

Arrangements of the gas puff port, the NBI heating, and the standard diagnostics in LHD have already been described elsewhere [5]. Ne gas is injected from the bottom port of the vacuum vessel with a typical flow rate of 5 Pa m^3/s. Total radiated power and energy stored in a plasma are measured by a resistive bolometer and a diamagnetic loop, respectively. Radial profiles of electron temperature (T_e) and density (n_e) are measured by a Thomson scattering diagnostic in a horizontally elongated cross-section with a spatial resolution of about 20 mm [8]. The electron density is calibrated using line-integrated density data of far-infrared (FIR) interferometer in a vertically elongated cross-section [9]. In this study, charge exchange spectroscopy (CXS) [10] was employed for the measurement of fully ionized Ne density. After the charge exchange recombination of the fully ionized Ne ions with fast hydrogen atoms in a vertically injected neutral beam, a subsequent visible line emission from H-like Ne X (n=11-10) is observed at 524.90 nm. Absolute ion density is calibrated using cross-section data in ADAS database [11].

VUV spectral lines from Ne ions are observed by a 2 m Schwob-Fraenkel grazing incidence spectrometer [12]. The spectrometer contains two microchannel plates with phosphor screens coupled to a 2048 channel silicon photodiode array detector via an imaging fiber optic conduit, which permits the simultaneous recording of spectra in two different

spectral bands. A grating is selectable from two with different groove densities (133.6 mm^{-1} and 600 mm^{-1}). In this study, Ne VI–VIII (n=2-3) lines in 8–12.5 nm and Ne III–VII (n=2-2) lines in 45–60 nm are measured using the 600 mm^{-1} and 133.6 mm^{-1} gratings, respectively. The frame rate of the detector was fixed at 50 ms, which is enough to follow the temporal evolutions. The line of sight of the spectrometer was fixed at the position passing through the plasma center in this experiment.

Figure 1 shows typical examples of the VUV spectra from (a) Ne VI–VIII (n=2-3) and (b) Ne III–VII (n=2-2) in Ne seeded discharges in LHD, measured by the 600 mm^{-1} and 133.6 mm^{-1} gratings, respectively. Spectral lines used for the analyses in this study are denoted by italic letters in Fig. 1, and are summarized in Table 1. In order to check the validity of the measured line intensities, the same spectral lines from the similar plasmas have been measured at several different positions over the detector by moving it. Consequently, it has been confirmed that the changes in sensitivity and hence line intensities across the detector are small enough, which indicates that the measured line intensity ratios would not be largely affected by the detector sensitivity.

Table 1 Spectral lines from Ne ions used for the analyses in this study.

	Ion	Transition	Wavelength (nm)
a	Ne VIII (Li-like)	$1s^2 2s\ ^2S$ - $1s^2 3p\ ^2P°$	8.81
b	Ne VIII (Li-like)	$1s^2 2p\ ^2P°$ - $1s^2 3d\ ^2D$	9.83
c	Ne VIII (Li-like)	$1s^2 2p\ ^2P°$ - $1s^2 3s\ ^2S$	10.3
d	Ne IV (N-like)	$2s^2 2p^3\ ^2D°$ - $2s2p^4\ ^2D$	47.0
e	Ne V (C-like)	$2s^2 2p^2\ ^3P$ - $2s2p^3\ ^3P°$	48.3
f	Ne IV (N-like)	$2s^2 2p^3\ ^4S°$ - $2s2p^4\ ^4P$	54.4
g	Ne V (C-like)	$2s^2 2p^2\ ^3P$ - $2s2p^3\ ^3D°$	57.2

3. Results

Figure 2 shows waveforms of parameters in a typical Ne seeded discharge together with

the temporal evolutions of the line intensities and intensity ratios for the three prominent Ne VIII lines listed in table 1 as ***a***–***c***. Bumps in NBI heating power (P_{NBI}) are due to the modulation of a vertical neutral beam required for charge exchange spectroscopy. After the Ne gas was puffed during 3.8–3.9 s with a flow rate of about 5 Pa m^3/s, total radiated power (P_{rad}) was almost doubled at 4.0 s and then decreased slowly without any degradation of the stored energy (W_p). Though the change in the ion saturation current of one of the divertor probes (I_{is}) happened to be unclear in this discharge, it slightly decreased at the same time. Indeed, a much clearer drop in I_{is} was usually observed in most of the other discharges. The three line intensity ratios are roughly constant throughout the discharge after the Ne seeding. They are roughly 0.75, 0.5, and 0.35 for ***a***/***b***, ***c***/***a***, and ***c***/***b***, respectively, with a scatter of ±0.05. These ratios were compared with the theoretical values derived from collisional-radiative models for Ne VIII using ADAS database [11] by a similar method employed in [7]. In general, population of an excited state of Z times charged ions (A^{Z+}) is written by the sum of the ionizing and recombining plasma components which are proportional to ground state populations of A^{Z+} and $A^{(Z+1)+}$, respectively. Because the fractional abundance of each Ne ion is unknown, the density ratio of Ne IX/Ne VIII is assumed to be 1–4, and charge exchange recombination processes are not included in the present calculation. Figure 3 shows the calculated intensity ratios plotted as functions of electron temperature. The solid and dash-dotted lines are the results for the Ne IX/Ne VIII density ratio of 1 and 4, respectively. In the modeling, an electron density of 2×10^{19} m^{-3} was assumed, though the intensity ratios have only very weak density dependences. The plots in figure 3 indicate that recombining components are dominant below 10 eV, while ionizing components are dominant above 40 eV, and both the components compete between 10 and 40 eV where the intensity ratios are dependent on the Ne IX/Ne VIII density ratio. The measured intensity ratios are indicated by horizontal dashed lines in Fig. 3. In principle, three electron temperatures derived from the

three intensity ratios should be consistent, and give a temperature region where Ne VIII emissions originate. Charge exchange recombination processes with neutral hydrogen, which are not included in Fig. 3, could contribute to the population density of the level $1s^2 3p$, the upper level of the line ***a***. Considering this effect, the intensity ratios ***a***/***b*** and ***c***/***a*** could be further increased and decreased, respectively, and a consistent solution may be found around 10–20 eV. Nevertheless, the effect of charge exchange processes should be further investigated in the future because it can make changes of the calculated intensity ratios.

Figure 4 shows density profiles of fully ionized Ne ions measured by CXS together with the electron temperature and density profiles measured by the Thomson scattering as functions of major radius (R) at 3.970, 4.271, and 4.471 s in the discharge shown in Fig. 2. Though electron temperature and density are almost unchanged during these periods, the fully ionized Ne density gradually increases in the core region. This implies that the inward flow and ionization of Ne ions still progressed after 4.3 s. The onset of the fully ionized Ne density is located around R = 4.6 m where the electron temperature is around 100 eV. This observation is consistent with the result of Ne VIII line intensity ratio analysis mentioned above in that the region where the electron temperature is around 10–20 eV is located around R = 4.69 m as shown in Fig. 4 (b).

We have measured temporal evolutions of the intensities of Ne IV–VIII lines listed in Table 1 using the 133.6 mm^{-1} grating in another Ne seeded discharge (not shown in the figure). Then we have attempted an intensity ratio analysis for the two pairs of Ne IV and Ne V lines in a similar way using the ADAS database, in which only the atomic data for the ionizing plasma component are available for Ne IV–V. The measured intensity ratios are 1.4 for Ne V (***d***/***f***) and 1.0 for Ne V (***e***/***g***), and almost unchanged during the discharge. The intensity ratios calculated for these line pairs are shown in Fig. 5 as functions of electron temperature together with the measured values indicated by dashed lines. As a result, it can be inferred that

an electron temperature range where Ne IV emits is around 30 eV corresponding to the position R = 4.67 m in Fig. 4. On the other hand, the measured ratio for Ne V cannot be explained by the modeling. However, it should be noted that there would be possible uncertainties in this modeling such as non-negligible recombining plasma component and unavailability of accurate atomic data due to more complex electronic configurations of Ne IV and Ne V.

4. Summary

We have carried out spectroscopic measurements of Ne IV–VIII line intensities in Ne seeded discharges to achieve the divertor detachment in LHD. We have compared the measured line intensity ratios of Ne VIII with those calculated from a collisional-radiative model. As a result, it can be inferred that the Ne VIII emissions would include the contribution from both of ionizing and recombining plasma components and originate from the region where the electron temperature is around 10–20 eV, provided that the present model does not include charge exchange recombination processes, whose effect will be investigated in the future. It has been confirmed that most of the fully ionized Ne exist in an inner region where the electron temperature is above 100 eV. Exact contributions from each charge state of Ne ions and intrinsic carbon ions should be investigated in the future because they still remain unclear in this study.

Acknowledgements

This work has been performed with the support and under the auspices of the budget NIFS10ULHH007 from the National Institute for Fusion Science.

References

[1] N. Asakura et al., Nucl. Fusion 49 (2009) 115010.

[2] M.L. Reinke et al., J.L. Terry, J. Nucl. Mater. 415 (2011) S340.

[3] A. Kallenbach et al., Plasma Phys. Control. Fusion 52 (2010) 055002.

[4] C. Giroud et al., Nucl. Fusion 53 (2013) 113025.

[5] S. Masuzaki et al., J. Nucl. Mater. 438 (2013) S133.

[6] T. Ishijima et al., Plasma Phys. Control. Fusion. 41 (1999) 1155.

[7] T. Nakano et al., J. Nucl. Mater. 438 (2013) S291.

[8] K. Narihara, I. Yamada, H. Hayashi and K. Yamauchi, Rev. Sci. Instrum. 72 (2001) 1122.

[9] T. Akiyama et al., Fusion Sci. Technol. 58 (2010) 352.

[10] M. Yoshinuma et al., Fusion Sci. Technol. 58 (2010) 375.

[11] H. P. Summers, The ADAS User Manual, version 2.6 (2004) http://www.adas.ac.uk.

[12] J. L. Schwob, A. W. Wouters, and S. Suckewer, Rev. Sci. Instrum. 58 (1987) 1601.

Figure captions

Fig. 1. Typical VUV spectra recorded in Ne seeded discharges in the wavelength regions of (a) 8.5–12.5 nm and (b) 45–60 nm measured by the 600 mm^{-1} and 133.6 mm^{-1} gratings, respectively. Spectral lines from Ne VI–VIII (n=2-3) are observed in (a) and Ne III–VII (n=2-2) in (b). The lines used for the analyses in this study are denoted by bold italic letters ***a***–***g*** and are summarized in table 1.

Fig. 2. Waveforms of various parameters in a typical Ne seeded discharge together with line intensities and intensity ratios of Ne VIII. Temporal evolutions of (a) total neutral beam heating power (P_{NBI}) and flow rate of Ne gas puff, (b) plasma stored energy (W_p) and total radiated power (P_{rad}), (c) line-averaged electron density ($<n_e>$) and ion saturation current (I_{is}) measured by one of the divertor probes, (d) intensities of spectral lines from Ne VIII listed in table 1 as ***a***–***c***, and (e) intensity ratios among these three lines.

Fig. 3. The calculated intensity ratios among three Ne VIII lines ***a***–***c*** in Table 1 as functions of electron temperature derived from a similar method employed in [7]. The solid and dash-dotted lines are the results for the Ne IX/Ne VIII density ratio of 1 and 4, respectively, and charge exchange recombination processes are not included. The measured intensity ratios are indicated by horizontal dashed lines.

Fig. 4. Spatial profiles of (a) fully ionized Ne density, (b) electron temperature (T_e), and (c) electron density (n_e) as functions of major radius (R) at 3.970, 4.271, and 4.471 s in the discharge shown in Fig. 2.

Fig. 5. The calculated intensity ratios for the two line pairs of Ne IV (***d***/***f***) and Ne V (***e***/***g***) as

functions of electron temperature. The measured ratios are indicated by horizontal dashed lines, and an electron temperature given by the measurement is denoted by a circle for Ne IV.

Fig. 1.

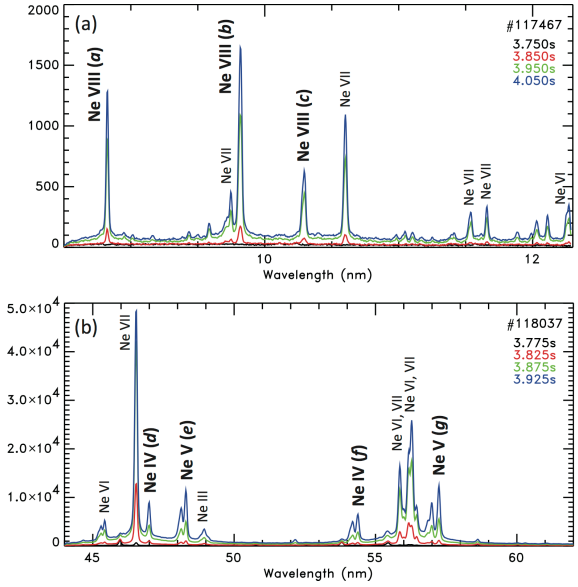
(a)
#117467
3.750s
3.850s
3.950s
4.050s
Ne VIII (a)
Ne VII
Ne VIII (b)
Ne VII
Ne VIII (c)
Ne VII
Ne VII
Ne VII
Ne VI
2000
1500
1000
500
0
10
12
Wavelength (nm)
(b)
#118037
3.775s
3.825s
3.875s
3.925s
Ne VI
Ne VII
Ne IV (d)
Ne V (e)
Ne III
Ne IV (f)
Ne VI, VII
Ne VI, VII
Ne V (g)
5.0×10^4
4.0×10^4
3.0×10^4
2.0×10^4
1.0×10^4
0
45
50
55
60
Wavelength (nm)

Fig. 2.

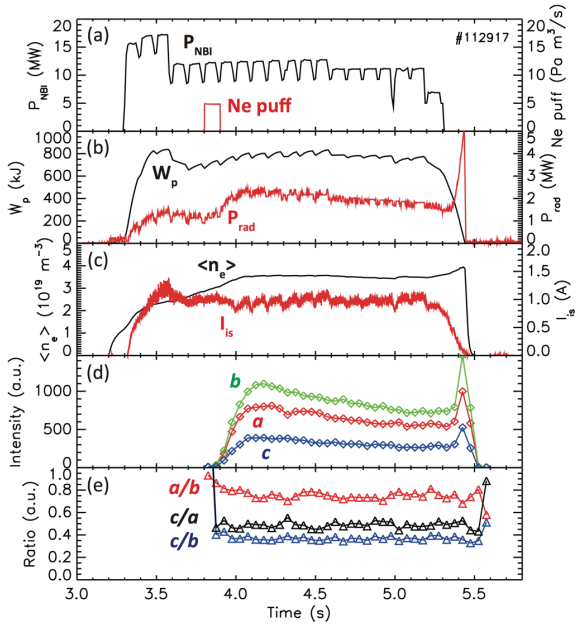
(a)
#112917
P_{NBI}
Ne puff
P_{NBI} (MW)
Ne puff (Pa m^3/s)
(b)
W_p
P_{rad}
W_p (kJ)
P_{rad} (MW)
(c)
<n_e>
I_{is}
<n_e> (10^{19} m^{-3})
I_{is} (A)
(d)
b
a
c
Intensity (a.u.)
(e)
a/b
c/a
c/b
Ratio (a.u.)
Time (s)

Fig. 3.

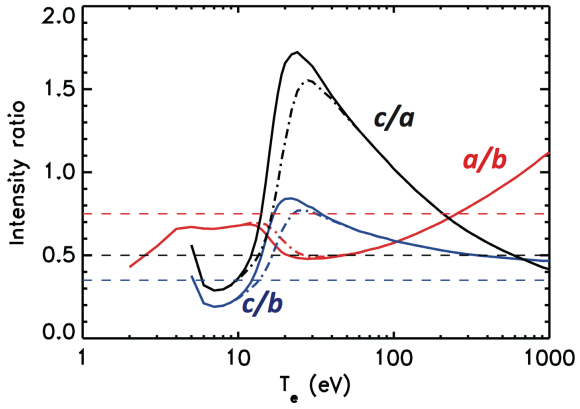

Fig. 4.

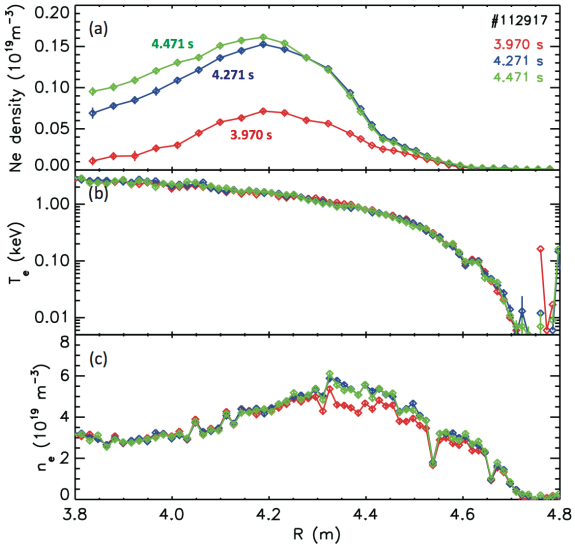
(a)
#112917
3.970 s
4.271 s
4.471 s
4.471 s
4.271 s
3.970 s
Ne density (10^{19}m^{-3})
0.20
0.15
0.10
0.05
0.00
(b)
T_e (keV)
1.00
0.10
0.01
(c)
n_e (10^{19} m^{-3})
8
6
4
2
0
3.8
4.0
4.2
4.4
4.6
4.8
R (m)

Fig. 5.